Civil Engineering Dimension
https://ced.petra.ac.id

Stress Analysis of Pin Connections in Steel Box Girder with the Unibridge System using Finite Element Model

Aprilia, A.S.[1], Awaludin, A.[1]*, Siswosukarto, S.[1], and Ngudiyono[2]
[1] Department of Civil and Environmental Engineering, Gadjah Mada University, Yogyakarta, INDONESIA
[2] Department of Civil Engineering, University of Mataram, Mataram, INDONESIA

DOI: https://doi.org/10.9744/ced.26.1.91-100

Article Info:
Submitted: Dec 25, 2023
Reviewed: Feb 16, 2024
Accepted: Feb 29, 2024

Keywords:
unibridge,
steel box girder,
pin connections,
finite element,
Von-Mises.

Corresponding Author:
Awaludin, A.
Department of Civil and Environmental Engineering, Gadjah Mada University, Yogyakarta, INDONESIA
Email: ali.awaludin@ugm.ac.id

Abstract

This study analyzes the Unibridge system, a modular steel box girder employing two pins for longitudinal connections, thereby expediting construction compared to traditional girders. A finite element model was developed to analyze the stress on these pins in a single-box girder with five segments and a reinforced concrete floor slab. Various loads were applied following the Indonesian bridge loading standard, SNI 1725:2016. The model considers operational load analysis and assumes full composite behaviour between the top flanges of the girder and the concrete floor slab. The results indicate that the Von-Mises stress on the pins reaches a maximum of 490.95 MPa under combined service loads, consistently remaining below the specified material yield stress limit of 1200 MPa. Consequently, the Demand Capacity Ratio (DCR) is 0.41. As a result, the Unibridge girder connection pins do not experience plastic deformation under the applied loads.

Introduction

Due to their inherent advantages, steel box girders have gained a reputation in bridge superstructures. The hollow steel box structure provides substantial torsional stiffness, ensuring it is well-suited particularly for application in bridges spanning long distances and featuring curves [1]. In addition, segmented girders undergo prefabrication before on-site assembly, typically using bolted or welded connections. Thus, the segmented steel box girder method reduces on-site construction time and minimizes traffic disruption [2,3].

The Unibridge, an innovative adaptation for steel box girders, originated from Matière, a French company [4], and had its initial application in Indonesia during the 2018 Teluk Lamong Terminal Flyover Project in Surabaya, East Java Province [5]. This innovative approach features a distinctive connection method between girders, utilizing pins for longitudinal connections and spacers bolted for transverse connections, as shown in Figure 1 [6]. In contrast to conventional girder connections, which often require specialized tools or welding, this system enables swift connection procedures without such requirements. Additionally, this system is adaptable, functioning as both temporary and permanent bridges due to its easy disassembly and reassembly. Installation can be adapted to available equipment, such as cranes or alternative launching methods.

This study evaluates the stress exerted on pins, an innovative component in longitudinal girder connections. Excessive stress, exceeding the material strength, poses a risk of structural failure. Furthermore, based on the gathered information, PT *Wijaya Karya Industri Konstruksi* collaborated with PT *Matiere Bridge Building Indonesia* to manufacture Unibridge girders. High-yield stress pins, rated at 1200 MPa, are specifically imported from PT Matiere

Note : Discussion is expected before July, 1st 2024, and will be published in the "Civil Engineering Dimension", volume 26, number 2, September 2024.
ISSN : 1410-9530 print / 1979-570X online
Published by : **Petra Christian University**

Bridge Building Indonesia [7]. A finite element model was developed for this study to simulate a single Unibridge girder span comprising five girder segments interconnected by pins. This simulation model incorporates a concrete slab on top of the steel girder to create a composite bridge structure. The data were collected from the Jogja-Bawen toll road project in the Yogyakarta Province, Indonesia, linking the city of Yogyakarta to Bawen. Some bridges in this project employ the Unibridge system. Subsequently, the finite element model underwent loading according to the Indonesian bridge loading standard, SNI 1725:2016 [8]. Previous studies [4,6] have only discussed the advantages of the Unibridge system without conducting numerical analysis. Therefore, this study aims to fill this gap by focusing on the stress analysis of pin connections in the Unibridge system. The study is expected to make a significant contribution to the advancement of bridge technology.

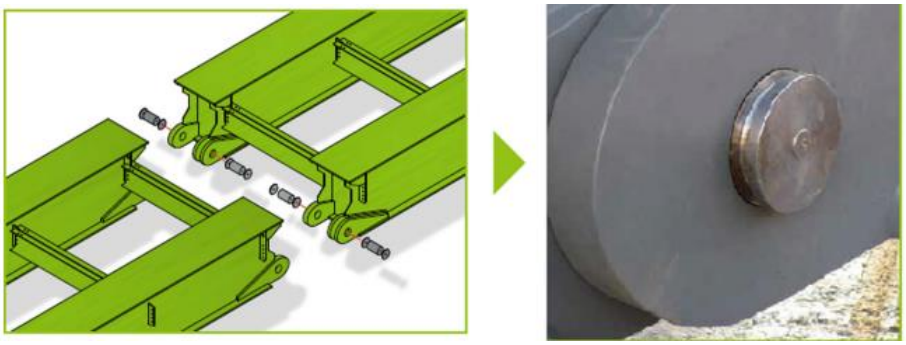

Figure 1. Unibridge Pin Connection [6]

Method

This study utilizes data from the Jogja-Bawen toll road project, which features the integration of the Unibridge system into its bridge structures. The bridge comprises three girder spans in the transverse direction, supporting a 12.7m wide concrete floor slab positioned atop the girders (Figure 2). The total longitudinal span of the girders extends to 57m (Figure 3). However, due to computational limitations, this study focused exclusively on modeling a single box girder span, covering a length of 57m, accompanied by a 4.25m wide concrete floor slab. This specific girder span consisted of five box girder segments, each spanning 11.4m and interconnected through pin connections (Figure 3). The modeling procedures were conducted using ABAQUS finite element software.

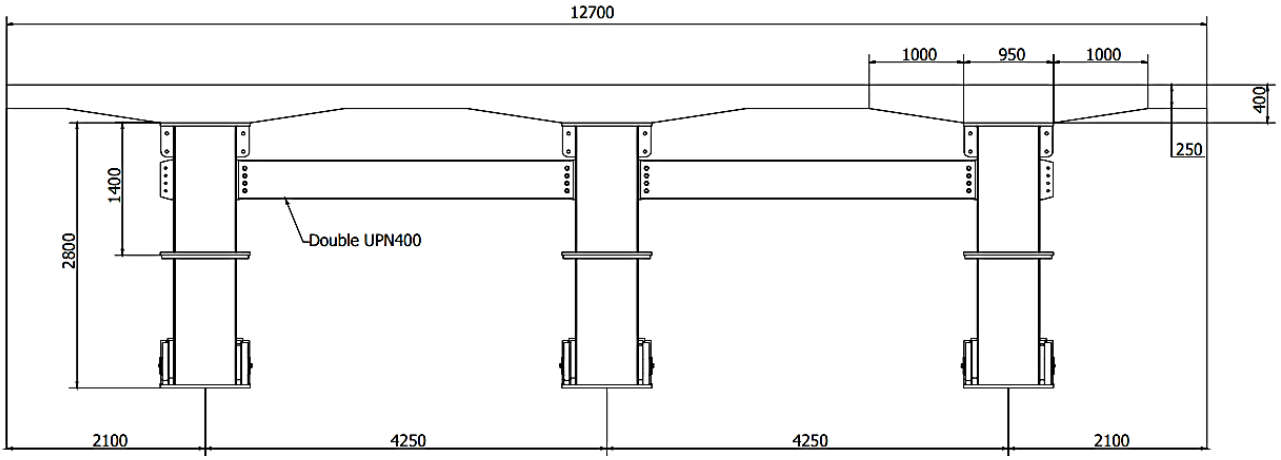

Figure 2. Cross-section of The Bridge (unit in mm)
Source: PT Adhi Karya (Persero) Tbk (2022 Dec)

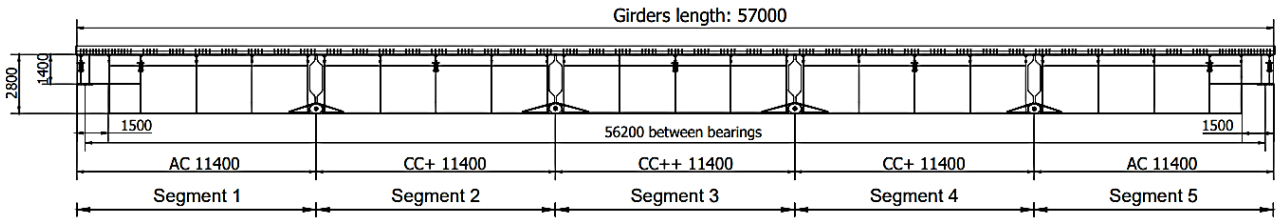

Figure 3. Longitudinal Section of The Bridge (unit in mm)
Source: PT Adhi Karya (Persero) Tbk (2022 Dec)

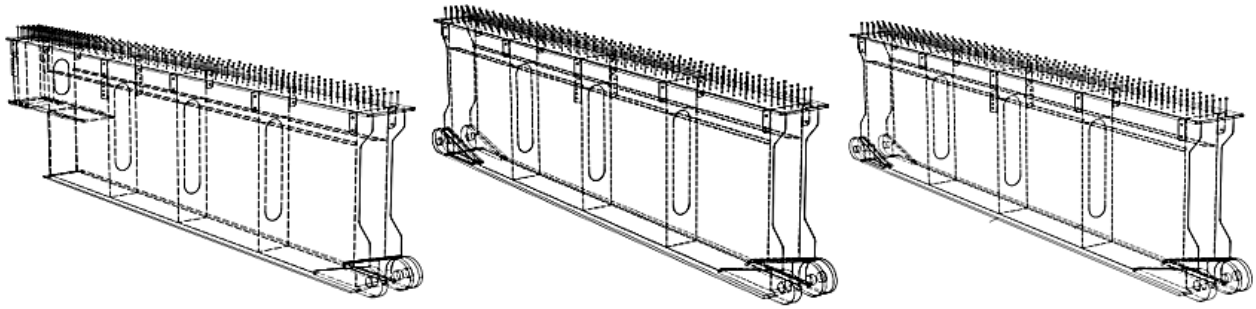

(a) (b) (c)

Figure 4. Box Girder: (a) Segments 1 and 5; (b) Segment 3; (c) Segments 2 and 4
Source: PT Adhi Karya (Persero) Tbk (2022 Dec)

Materials and Dimensions

The girders are primarily made of steel, whereas the bridge floor slab is composed of reinforced concrete. Each material possesses distinct properties, which are summarized in Table 1. Additionally, Table 2 provides comprehensive details about the materials and dimensions of each girder component, including the top flange, bottom flange, web, diaphragm, ear, and pin. Figure 4 shows different dimensions within the five segments constituting the box girder. These segments can be categorized into three distinct types: a) girder segment 1, identical to segment 5, represents the end sections of the girder; b) girder segment 2, similar to segment 4; and c) segment 3, positioned at the mid-span of the bridge. The differences among these categories are primarily attributed to the dimensions and material properties of the top flange, bottom flange, web, and ear, as outlined in Table 2.

Table 1. Materials Properties of Steel and Concrete

Material	Properties	Value	Reference
Steel	Modulus of elasticity	200000 MPa	SNI 1729:2020 [9]
	Poisson's ratio	0.3	Coronado (2010) [10]
	Density	7850 kg/m^3	PT Adhi Karya (Persero) Tbk
Concrete	Concrete compressive strength	30 MPa	PT Adhi Karya (Persero) Tbk
	Density	2400 kg/m^3	SNI 2847:2019 [11]
	Modulus of elasticity ($4700\sqrt{fc'}$)	25742.96 MPa	SNI 2847:2019 [11]
	Poisson's ratio	0.2	Coronado (2010) [10]

Table 2. Materials and Dimensions of the Box Girder (PT Adhi Karya (Persero) Tbk)

Descriptions	Materials	Thickness (mm)	Segment	f_y (MPa)	f_u (MPa)
Top Flange	JIS SM490YB	35	1,5	355	490
	JIS SM570	35	2,3,4	450	570
Bottom Flange	JIS SM490YB	30	1,5	355	490
	JIS SM570	40	2, 4	450	570
	JIS SM570	44	3	430	570
Web	JIS SM490YB	12	1,5	365	490
	JIS SM570	12	2,3,4,	460	570
Diaphragm	JIS SM490YB	18	1,2,3,4,5	365	490
Male Ear Spacer	EN S460ML	110	1,2,4,5	385	490
Female Ear Spacer	EN S355ML	117	1,2,4,5	295	450
Male Ear Spacer	EN S460ML	140	2,3,4	385	490
Female Ear Spacer	EN S355ML	147	2,3,4	295	450
Female Ear	EN S460ML	70	1,2,3,4,5	385	490
Pin	S1200	147	1,2,3,4,5	1200	1400

Modeling Procedure

The developed finite element model as depicted in Figure 5 is a three-dimensional representation of Unibridge system and comprising of a single-span box girder, a concrete slab floor, and two pin connections positioned at four specific locations. This model is designed to simulate the operational stage of the bridge, assuming the establishment of composite action between the top flange of the girder and the concrete floor slab. Despite the presence of shear connectors shown in Figure 4, which connect the top flange of the girder to the concrete slab, these connectors were

excluded from the model due to computational constraints associated with the computer capability. This study assumes complete composite behavior between the top flange of the girder and the concrete slab, considering any displacement or deformation between the materials as negligible and thus disregarding them. Consequently, a tie constraint interaction was adopted in the model assembly process to link these two elements, preventing any relative movement between them [12].

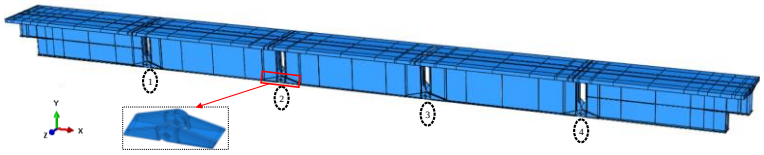

Figure 5. 3D Model of Pin in ABAQUS

Each ear is equipped with a hole of 149 mm in diameter for inserting a pin with a diameter of 147 mm, thus creating a gap. However, this gap is discounted in the applied model, assuming a snug fit for the pin. This decision is based on the calculation that the hole diameter ratio to the pin diameter is approximately 101.36%, falling within the 110% limit. Consequently, this exclusion does not compromise the strength of the ear [13]. In pin connections, the contact between the ear hole's surface and the pin generates friction, necessitating a friction coefficient to characterize this interaction. The friction coefficient typically ranges between 0.15 and 0.2 for steel surfaces without lubrication. With lubrication, this value diminishes to a range between 0.05 and 0.15 [14]. Previous finite element study [14] demonstrates that stress at the contact areas increases with an escalation in the coefficient of friction. It is attributed to heightened friction between contacting surfaces, hindering relative movement and resulting in a reduced contact area. Notably, in this study, lubrication is employed in the pin connection, setting the friction coefficient between the ear hole's surface and the pin at 0.14 [14], which is subsequently applied to the finite element modeling of the area in Figure 6.

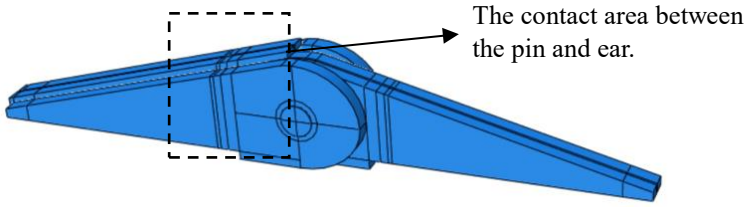

Figure 6. Pin Connection

The pin is equipped with restraining elements or pinheads at both ends, designed to prevent disengagement from the connection. It is noteworthy that current code specifications need regulations addressing these elements, and they are frequently overlooked in the design process [15]. Consequently, in this model, the restraining elements on both sides are not taken into consideration.

Bridge Loading

The applied load on the bridge model follows Indonesian loading standard SNI 1725:2016 [8], a standard that governs the specifications of loads to be considered in bridge design in Indonesia. These loads include dead load (MS), additional dead load (MA), lane load (TD), truck Load (TT), brake force (TB), wind load (EW_L and EW_s), and temperature load (ET).

Mesh Convergence

The concept of finite element analysis involves dividing complex structures into smaller elements, a process commonly known as discretization [16] The size of these elements directly impacts the accuracy of analysis results; smaller elements offer greater precision but demand longer analysis times and more computational resources. Therefore, ensuring mesh convergence is crucial for approximating precise solutions while optimizing computer efficiency. In pin connection modelling, two different mesh sizes are used to optimize computational efficiency. Specifically, a smaller mesh size is applied at the pin connections compared to other sections. Figure 7 shows the meshing results obtained through a "trial and error" process, wherein the stress at the connection stabilizes with a mesh size of 0.004m for the pin and ear hole in contact with the pin, while the other parts have a mesh size of 0.07m.

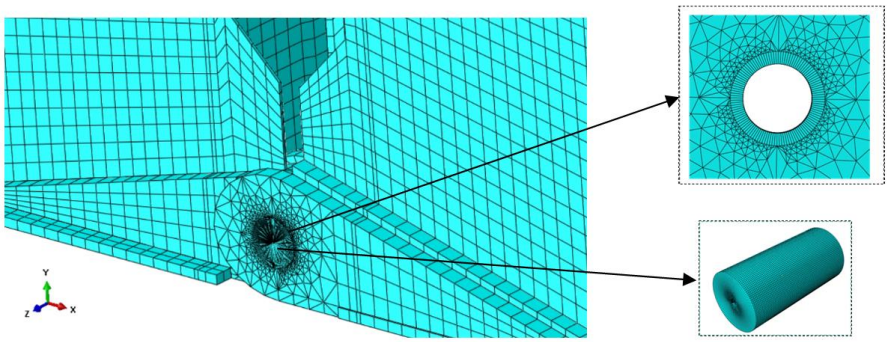

Figure 7. Meshing of Pin Connection

Failure Analysis

The stress analysis of pin connections employs Von-Mises stresses, which is suitable for the ductile nature of the steel used, as it exhibits yielding behaviour. The Von-Mises theory is particularly appropriate for ductile materials, indicating material safety when the maximum distortion energy per unit volume remains below the threshold that induces yield conditions in the material [17]. Equation 1 describes the Von-Mises stress equation, where σ_1, σ_2, and σ_3 denote the principal stress values acting on each axis, and σ_y represents the yield stress limit of the material. Material failure occurs when the stress exceeds the yield stress limit.

$$(\sigma_1-\sigma_2)^2 + (\sigma_2-\sigma_3)^2 + (\sigma_1-\sigma_3)^2 = 2\sigma_y^2 \quad (1)$$

Results and Discussion

Bridge Deflection

The assessment of the bridge model's deflection aimed to validate its compliance with the anticipated deflection induced by the vehicular load (lane load). The recorded deflection within the bridge model measured 53.75 mm, as shown in Figure 8, while the deflection design was 53 mm. This slight deviation of 1.5% indicates that the model's deflection follows closely to the specified standard, affirming the conformity of the bridge model – including the girders and the superimposed concrete slab – with the original design parameters.

Furthermore, a deflection examination was conducted to ensure that it conforms with the maximum deflection limit outlined in accordance with AASHTO 2017 regulations [18]. These regulations specify that for bridges lacking of sidewalks, the maximum deflection caused by vehicular loads is determined as L/800, with L representing the bridge span's length [18]. This examination ensures that the observed deflection remains below the prescribed maximum limit of 0.07025 m, in accordance with regulation.

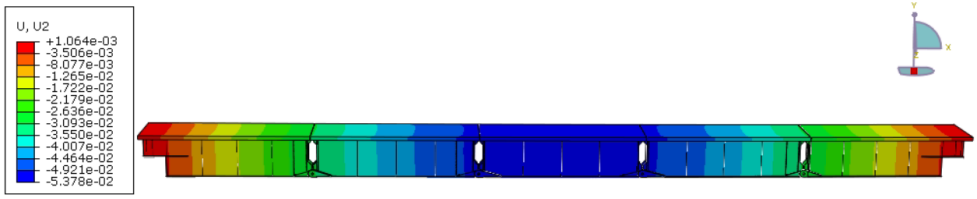

Figure 8. The Deflection Results in the Bridge Model due to Lane Load (unit in meters)

Stress Ratio of Girder Components

The assessment involves the analysis of the maximum normal stress (S_{11}) and shear stress (S_{12}) at the web, ear, and pin to characterize the overall behavior of the girder structure. These stress values are then compared with the yield stress (f_y) of the material to determine the Demand Capacity Ratio (DCR) of the stress values. This evaluation is crucial as the permissible DCR limit on steel under maximum service loads is set at 0.66 [9]. Tables 3 and 4 present the DCR for the web and ear across segments 1, 2, and 3. Meanwhile, Table 5 illustrates pin 1 connecting girder segment 1 and segment 2, and pin 2 linking girder segment 2 and segment 3. Segments 4 and 5 were excluded due to their structural similarity to segments 1 and 2. The resulting DCR in Table 3 indicates that the highest stress occurs in the normal stress (S_{11}), with the web having a maximum DRC value of 0.433 in segment 3. Meanwhile, Table 4

shows that the ear has a maximum DCR value of 0.598, also occurring in segment 3, and Table 5 demonstrates that the pin has a maximum DCR value of 0.250 at pin 2. Therefore, all the DCR results indicate that the stress in the box girder components remains below the permissible steel stress.

Table 3. Stress Ratio on The Girder Web due to Combination of Service Loads

No.	Girder Segments		Load Combination							
			Service 1 (MS+MA+TD+TB+ 0.3EWs+EWL+1.2ET)		Service 2 (MS+MA+1.3TD+ 1.3TB+1.2ET)		Service 3 (MS+MA+0.8TD+ 0.8TB+1.2ET)		Service 4 (MS+MA+0.7EWs +1.2ET)	
			Max. Stress	DCR	Max. Stress	DCR	Max. Stress	DCR	Max. Stress	DCR
1	Segment 1	S_{11}	99.01	0.271	99.82	0.273	84.86	0.232	78.67	0.216
		S_{12}	45.47	0.125	47.87	0.131	39.49	0.108	30.70	0.084
2	Segment 2	S_{11}	153.52	0.334	166.91	0.363	139.73	0.304	100.35	0.218
		S_{12}	36.38	0.079	38.89	0.085	32.26	0.070	24.53	0.053
3	Segment 3	S_{11}	179.82	0.391	**199.34**	**0.433**	162.75	0.354	106.72	0.232
		S_{12}	25.82	0.056	29.08	0.063	22.37	0.049	13.32	0.029

Table 4. Stress Ratio on the Pin Ear due to Combination of Service Loads

No.	Girder Segments		Load Combination							
			Service 1 (MS+MA+TD+TB+ 0.3EWs+EWL+1.2ET)		Service 2 (MS+MA+1.3TD+ 1.3TB+1.2ET)		Service 3 (MS+MA+0.8TD+ 0.8TB+1.2ET)		Service 4 (MS+MA+0.7EWs +1.2ET)	
			Max. Stress	DCR	Max. Stress	DCR	Max. Stress	DCR	Max. Stress	DCR
1	Segment 1	S_{11}	155.55	0.404	161.79	0.420	132.20	0.343	108.34	0.281
		S_{12}	57.90	0.150	61.42	0.160	50.77	0.132	39.35	0.102
2	Segment 2	S_{11}	185.68	0.482	201.62	0.524	168.27	0.437	120.65	0.313
		S_{12}	62.30	0.162	67.28	0.175	55.62	0.144	40.40	0.105
3	Segment 3	S_{11}	211.00	0.548	**230.17**	**0.598**	190.61	0.495	131.55	0.342
		S_{12}	80.66	0.210	88.01	0.229	72.26	0.188	49.03	0.127

Table 5. Stress Ratio on the Pin due to Combination of Service Loads

No.	Location of Pins		Load Combination							
			Service 1 (MS+MA+TD+TB+ 0.3EWs+EWL+1.2ET)		Service 2 (MS+MA+1.3TD+ 1.3TB+1.2ET)		Service 3 (MS+MA+0.8TD+ 0.8TB+1.2ET)		Service 4 (MS+MA+0.7EWs+ 1.2ET)	
			Max. Stress	DCR	Max. Stress	DCR	Max. Stress	DCR	Max. Stress	DCR
1	Pin 1	S_{11}	134.18	0.112	145.91	0.122	120.63	0.101	85.91	0.072
		S_{12}	10.58	0.009	11.62	0.010	8.26	0.007	4.83	0.004
2	Pin 2	S_{11}	272.79	0.227	**300.58**	**0.250**	246.88	0.206	165.27	0.138
		S_{12}	60.46	0.050	66.57	0.055	53.94	0.045	35.84	0.030

Von-Mises Stress at Pin Connections

The application of various loads outlined in SNI 1725:2016 [8] to the numerical model induces stress responses throughout the bridge structure, particularly within the pin connections. Notably, in the Unibridge model, the pin material exhibits the highest yield stress among the structural elements, reaching 1200 MPa. However, potential risks of pin failure, such as breakage due to stress exceeding the material's strength or yield stress limit, require careful consideration [19]. These failures might arise from heightened contact stresses, leading to surface wear between the pins [14]. Consequently, this study aims to present the stress analysis outcomes concerning the pins resulting from applied loads.

Several previous studies [19-24] have emphasized stress analysis in pin connections. However, the primary focus of these studies has been on examining the behaviour of connection plates, with relatively few addressing the potential failure modes associated specifically with the pins. This difference arises from the need for more experimental data, particularly since the widespread adoption of high-strength steel. Consequently, it is reasonable to suggest that the dominance of the pin element within the connection has diminished [15,24]. Moreover, finite element-based studies

on pin connections often focus solely on the plates to be joined and the pins. Typically, one end of the plate serves as a support, while the opposing end is subjected to tensile forces, as described in previous studies [22]. However, in this investigation, the modelling covers all elements constituting the bridge structure. This comprehensive approach aims to simulate the system's behaviour under conditions that more closely resemble actual scenarios, diverging from the conventional focus solely on the pin connection.

As depicted in Table 6, the analysis reveals that the maximum Von-Mises stress encountered by the pin is induced by the dead load, measuring about 202.80 MPa. Notably, this result signifies that the pin experienced stresses remain well below the material's yield stress limit for the pin, which is set at 1200 MPa. The stress distribution across the pin due to various loads applied on the bridge model is visually illustrated in Figures 9 through 16. These pictures explain that the primary stress concentration on the pin predominantly occurs within the pin-end region, whereas relatively lower stress levels apparent at the pin's centre. The results of stress distribution in this study are closely similar to the previous study by Vican et al. [24].

Table 6. Von-Mises Stress Results on The Pin for Each Load

Load	Stress (MPa)
Dead Load (MS)	202.80
Additional Dead Load (MA)	59.79
Lanes Load (TD)	175.60
Wind Load on the structure (EW_s)	3.81
wind load of vehicles (EW_L)	17.49
Braking force (TB)	0.007
Temperature (ET)	0.056
Truck load (TT)	75.60

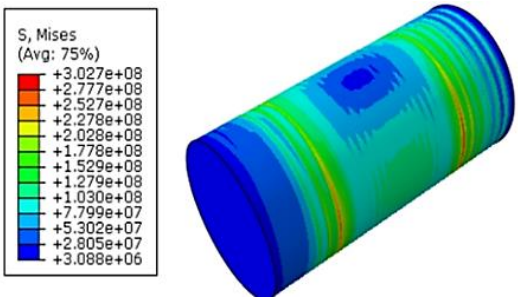

Figure 9. Stress Distribution on the Pin due to Dead Load

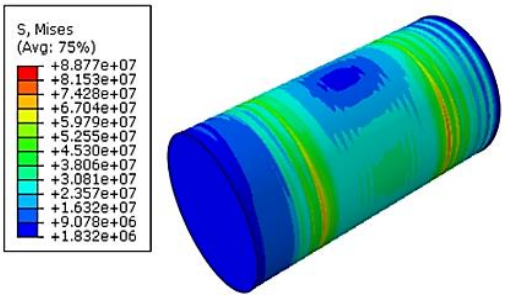

Figure 10. Stress Distribution on the Pin due to Additional Dead Load

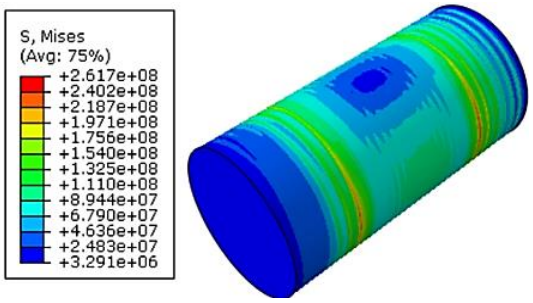

Figure 11. Stress Distribution on the Pin due to Lane Loads

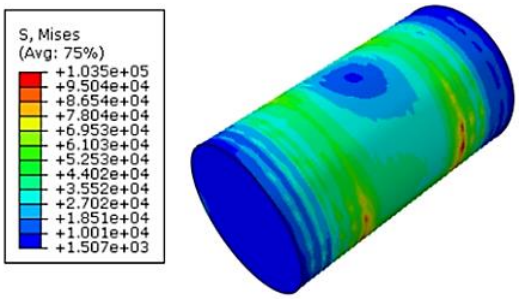

Figure 12. Stress Distribution on the Pin due to Braking Force

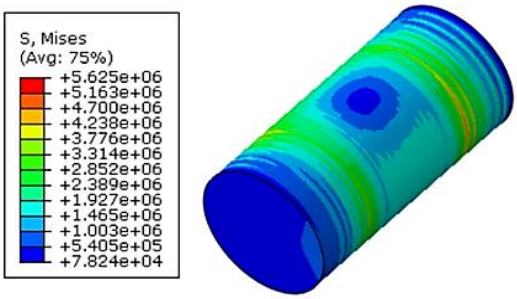

Figure 13. Stress Distribution on the Pin due to The Wind Load of Vehicles

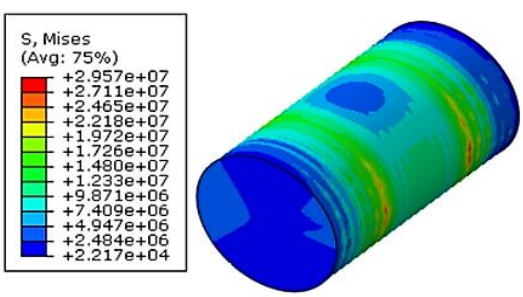

Figure 14. Stress Distribution on the Pin due to Wind Load on The Structure

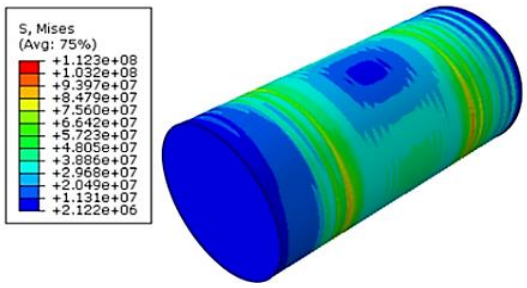

Figure 15. Stress Distribution on The Pin due to Truck Load

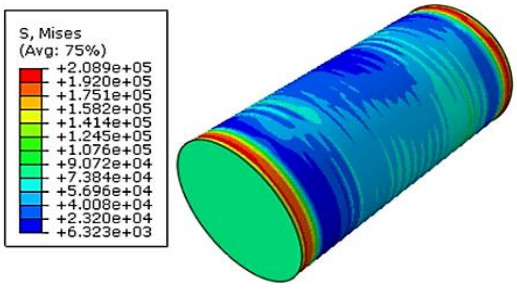

Figure 16. Stress Distribution on The Pin due to Temperature

After determining the stress induced by each load, the subsequent step involves evaluating the stress on the pin resulting from a combination of service loads in accordance with the specifications outlined in SNI 1725:2016 [8]. It is noteworthy that the specific pin under study is located at position 2. Results of finite element analysis indicate that the pin experiences the highest Von-Mises stress resulting from the combination of service loads. In contrast, the pin at Location 4 shows the lowest Von-Mises stress attributed to the service load combination. This difference arises from its proximity to the roll support, resulting in lower stress compared to the pin near the hinge support (pin location 1). Consequently, the relevant pins considered for assessment, as detailed in Table 7, are those situated at location 2.

Table 7. Von-Mises Stress Results on the Pin using Load Combinations

Load Combination	Von-Mises Stress (MPa)	f_y (MPa)
Service 1 (MS+MA+TD+TB+0.3EWs+EWL+1.2ET)	447.32	1200
Service 2 (MS+MA+1.3TD+1.3TB+1.2ET)	**490.95**	1200
Service 3 (MS+MA+0.8TD+0.8TB+1.2ET)	403.14	1200
Service 4 (MS+MA+0.7EWs +1.2ET)	274.90	1200

As shown in Table 7, the highest stress recorded on the pin under service load combination 2 is 490.95 MPa. This stress level is well below the material's yield stress limit, set at 1200 MPa, resulting in a DCR of 0.41. Consequently, the pin stress remains within its elastic limit, ensuring it does not exceed the plastic phase. Thus, even after deformation, the pin retains the ability to revert to its original shape once the applied load is removed.

Furthermore, as part of the pin stress analysis, the finite element analysis also evaluates the stress on the pin ear interacting with pin location 2. Table 8 displays the maximum Von-Mises stress observed on the pin ear for individual loads, while Table 9 illustrates the Von-Mises stress on the pin ear induced by the combined service load. Significantly, these findings indicate that the stress experienced by the pin ear remains below the material's yield stress threshold, set at 385 MPa. Hence, the applied load has not triggered plastic deformation in the ear.

Table 8. Von-Mises Stress Results on The Ear for Each Load

Load	Stress (MPa)
Dead Load (MS)	**132.10**
Additional Dead Load (MA)	38.85
Lanes Load (TD)	109.30
Wind Load on the structure (EW_s)	2.59
wind load of vehicles (EW_L)	14.72
Braking force (TB)	0.006
Temperature (ET)	0.003
Truckload (TT)	67.78

Table 9. Von-Mises Stress Results on The Ear-Using Load Combinations

Load Combination	Von-Mises Stress (MPa)	f_y (MPa)
Service 1 (MS+MA+TD+TB+0.3EWs+EWL+1.2ET)	287.27	385
Service 2 (MS+MA+1.3TD+1.3TB+1.2ET)	**313.05**	385
Service 3 (MS+MA+0.8TD+0.8TB+1.2ET)	258.40	385
Service 4 (MS+MA+0.7EWs +1.2ET)	181.26	385

Fatigue S-N Curve of Steel at Pin Connections

The S-N curve, commonly known as the Wohler diagram, visually represents the relationship between fatigue strength and the number of load cycles [25]. When portrayed logarithmically, Figure 17 typically illustrates the S-N

curve for steel materials. In this representation, the applied stress is characterized by the ratio of tensile stress to the ultimate stress of the utilized steel material.

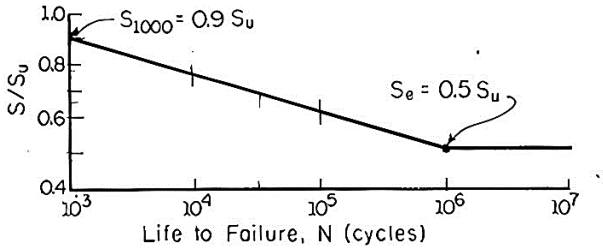

Figure 17. Generalized S-N Curve on a Log-log Plot for Wrought Steels [25]

In the AASHTO 2012 [26] specifications, there are two fatigue combinations: 1) Fatigue I, corresponding to a load factor of 1.5 times the vehicle load (S_{LL}), and 2) Fatigue II, with a load factor of 0.75 times the vehicle load (S_{LL}). Consequently, in this investigation, the Fatigue I combination is employed, as it results in the maximum stress. The stress value resulting from the Fatigue I combination is presented in Table 10. These values listed in Table 10 facilitate the observation of the S-N curve on the connection in Figure 18, indicating that the connection exhibits infinite life with a substantial number of cycles.

Table 10. Values for S-N Curves at Pin Connections

Element	S_u (MPa)	S_{LL} (MPa)	$S_{fatigue\ I}$ (MPa)	S/S_u	N (cycles)
Pin	1400	107.40	166.47	0.119	4E+15
Ear	490	79.12	122.64	0.250	6E+11

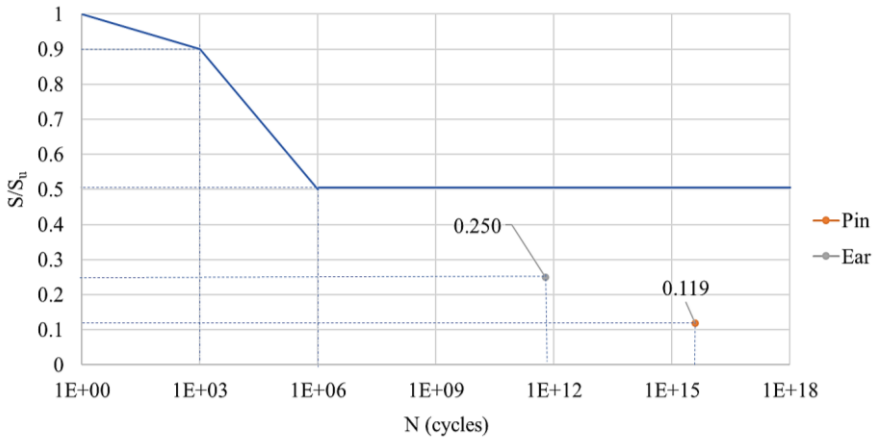

Figure 18. The S-N Curve of Pin Connections [25]

Conclusions

The finite element analysis underlines the pins' capability, which serve as longitudinal connectors in steel box girder structures employing the Unibridge system, to withstand loads according to the Indonesian Bridge standards, SNI 1725:2016. Throughout various load combinations in the finite element model, comprising dead load, additional dead load, lane load, brake force, wind load, truckload, and temperature, the Von-Mises stress within the pin material consistently remains well below the yield stress limit, set below 1200 MPa. Furthermore, the utilization of stress results from different loads to formulate service load combinations, as outlined in SNI 1725:2016, reveals that the Von-Mises stress consistently remains significantly lower than the yield stress. Specifically, it reaches 490.95 MPa with a DCR of 0.41. However, it is essential to acknowledge that this study does not incorporate the modelling of shear connectors on steel girders, which are crucial to maintain the connection with concrete slabs. Consequently, the bridge model constructed herein is assumed fully composite, necessitating further evaluation in this specific aspect.

Acknowledgment

The authors extend their gratitude to PT Adhi Karya (Persero) Tbk for their invaluable support in supplying data and granting access to observe the on-site construction of the Unibridge.

References

1. Abedi, H.A.O., Rasheed, M.M., and Alwaili, R.A.A., The Effect of Interior Stiffeners on the Flexural Behavior of Concrete-filled Steel Tube Composite Box Girders, *Engineering, Technology and Applied Science Research*, *13*(4), 2023, pp. 11412–11419. DOI: 10.48084/etasr.6088.
2. Yen, B.T., *Strength of Rectangular Composite Box Girders: Recommendations for Design of Composite Box Girders (Final Report)*, Fritz Laboratory Reports, 1982.
3. Hassan, E.M. and Mahmoud, H., Analytical and Numerical Behavior of Double Composite Steel Bridges, *Journal of Bridge Engineering, 28*(1), 2023. DOI: 10.1061/(asce)be.1943-5592.0001972.
4. Eaethk, J. and Mpaerhtfmg, A., Unibridge®: Construire et Reconsteuire, *Eiffage Construction Durable*, 2012.
5. PT Wijaya Karya (Persero) Tbk, *Wika Pelindo III Sinergi Bangun Jalur Akses Menuju Terminal Teluk Lamong,* Press Release, 2018.
6. Matiere, N, Ung, Q.H., and Nicolaudie, P.A., Unibridge®: A New Concept in Prefabricated Modular Bridge, *Lecture Notes in Civil Engineering*, *8*, 2018, pp. 981–987. DOI: 10.1007/978-981-10-6713-6_98.
7. Sukmawijaya, A., *Wikon Gandeng Perusahaan Prancis Ekspor Baja Jembatan ke Filipina*, April 2019., Retrieved from Kumparan Bisnis: https://kumparan.com/kumparanbisnis/1qwra8Laxxd?utm_source=Desktop&utm_medium=copy-to-clipboard&shareID=4FmNGzGlcIgH, Accessed 18 December 2023.
8. Badan Standardisasi Nasional, *SNI 1725:2016 Pembebanan untuk Jembatan*, 2016, [Online]. Available: www.bsn.go.id
9. Badan Standardisasi Nasional, *SNI 1729:2020 Spesifikasi untuk Bangunan Gedung Baja Struktural*, 2020.
10. Coronado, C.A. and Lopez, M.M., Numerical Modeling of Concrete-FRP Debonding Using a Crack Band Approach, *Journal of Composites for Construction*, *14*(1), 2010, pp. 11–21. DOI: 10.1061/(asce)cc.1943-5614.0000044.
11. Badan Standardisasi Nasional, *SNI 2847:2019 Persyaratan Beton Struktural untuk Bangunan Gedung*, 2019.
12. Dassault Systemes, *Getting Started with Abaqus: Keywords Edition*, 2014.
13. Duerr, D., *ASME BTH-1 Pinned Connection Design Provisions*, 2008. DOI: 10.1061/ASCE1084-0680200813:253.
14. Li, Y., Huang, R., Zhao, S., and Wang, J., Contact Pressure Analysis of Pin-Loaded Lug with Clearance, *Advances in Mechanical Engineering*, *14*(6), 2022. DOI: 10.1177/16878132221107475.
15. Conde, J., da Silva, L.S., Tankova, T., Simões, R., and Abecasis, T., Design of Pin Connections Between Steel Members, *Journal of Constructional Steel Research*, *201*, 2023. DOI: 10.1016/j.jcsr.2022.107752.
16. Logan, D.L., *A First Course in the Finite Element Method*, 2017.
17. Beer, F., *Mechanics of Materials*, Mcgraw-Hill Education, New York, 2009.
18. American Association of State Highway and Transportation Officials, *AASHTO LRFD Bridge Design Specifications*, Part I: Sections 1-6, 2017.
19. Ekvall, J.C., Static Strength Analysis of Pin-Loaded Lugs, *Journal of Aircraft, 23*(5), 1986, pp. 438–443. DOI: 10.2514/3.45326.
20. Wearing, J.L., Arnell, P.P, and Patterson, C., A Study of the Stress Distribution in a Lug Loaded by a Free Fitting Pin, *Journal of Strain Analysis for Engineering Design, 20*(4), 1985, pp. 217–224. DOI: 10.1243/03093247V204217.
21. Lin, S., Hills, D.A., and Nowell, D., Stresses in a Flat Plate due to a Loose Pin Pressing Against a Cracked Hole, *Journal of Strain Analysis*, *32*(2), 2015.
22. Pedersen, N.L., Stress Concentration and Optimal Design of Pinned Connections, *Journal of Strain Analysis for Engineering Design*, *54*(2), 2019, pp. 95–104. DOI: 10.1177/0309324719842766.
23. Grant, R.J. and Flipo, B.C.D., Parametric Study of the Elastic Stress Distribution in Pin-Loaded Lugs Modelled in Two and Three Dimensions and Loaded in Tension, *Journal of Strain Analysis for Engineering Design*, *44*(6), 2009, pp. 473–489. DOI: 10.1243/03093247JSA501.
24. Vičan, J. and Farbák, M., Analysis of High-Strength Steel Pin Connection, *Civil and Environmental Engineering*, *16*(2), 2020, pp. 276–281. DOI: 10.2478/cee-2020-0027.
25. Bannantine, J., Corner, J.J., and Handrock, J.L., *Fundamental of Metal Fatigue Analysis*, New Jersey: Prentice Hall, 1989.
26. American Association of State Highway and Transportation Officials, *AASHTO LRFD Bridge Design Specifications*, Customary U.S. Units, American Association of State Highway and Transportation Officials, 2012.